

Complex Impedance Measurement Applied to Short-Time Contact Between Colliding Steel Surfaces

Takahiro Nihira · Kazuyoshi Manabe ·
Chiharu Tadokoro · Shingo Ozaki ·
Ken Nakano

Received: 7 October 2014 / Accepted: 8 January 2015 / Published online: 30 January 2015
© Springer Science+Business Media New York 2015

Abstract The complex impedance method was developed for measuring the transient behaviors of short-time contacts between colliding steel surfaces, by using an alternating current circuit with a high frequency of 500 kHz at a high sampling rate of 20 MHz. The method was applied to estimate the lubrication effects of simple test lubricants acting at a short-time contact with a duration of 110 μ s occurring between a free-falling steel ball and a stationary steel plate, where to minimize the hydrodynamic lubrication effect, the test lubricant was provided on the steel plate as a homogeneous thin film with a thickness of 30 μ m. An advantage of the method is in the detection of the beginning and end of the contact. Particularly for wet conditions, although they were apparently unclear in the output voltage signal from the circuit, the modulus of the complex impedance detected them with high accuracy. In addition, using the modulus and argument of the complex impedance, the metallic contact ratio and residual film thickness at the short-time contact can be estimated quantitatively. By using the metallic contact duration determined by the metallic contact ratio, the differences in the boundary lubrication effects were quantified for the selected base oils (i.e., *n*-decane, *n*-dodecane, *n*-tetradecane, and *n*-hexadecane) and

the 30-mM oleic acid solutions dissolved in the base oils at the short-time contact, although the differences in the lubricants did not change the shape of the plastic indentation formed on the steel plate.

Keywords Collision · Lubrication · Metallic contact · Residual film · Complex impedance

List of symbols

a	Dimensionless coefficient
b	Dimensionless coefficient
C_f	Capacitance of lubricant film
d	Thickness of lubricant film
d_{\min}	Residual film thickness
e_r	Coefficient of restitution
f	Frequency
f_0	Frequency of alternator
\bar{F}	Mean contact force
g	Gravitational constant
h_0	Initial height of ball
I_1	Amplitude of I_1^*
I_1^*	Alternating current
j	Imaginary unit
L	Inductance
m	Mass of ball
\bar{P}	Mean contact pressure
p_p	Plastic flow pressure
r	Radial position
R	Resistance of fixed resistor
R_m	Resistance of metallic contact
S	Apparent contact area
S_f	Area covered with lubricant film
S_m	Area of metallic contact
$S_{m,\max}$	Maximum of S_m

T. Nihira · K. Manabe · K. Nakano (✉)
Faculty of Environment and Information Sciences, Yokohama
National University, 79-7 Tokiwadai, Hodogaya,
Yokohama 240-8501, Japan
e-mail: nakano@ynu.ac.jp

C. Tadokoro
Department of Mechanical Engineering, Tokyo University of
Science, 6-3-1 Niijuku, Katsushika, Tokyo 125-8585, Japan

S. Ozaki
Faculty of Engineering, Yokohama National University, 79-5
Tokiwadai, Hodogaya, Yokohama 240-8501, Japan

$S_{m,SP}$	S_m during stable period
S_{m0}	S_m for dry condition
$S_{m0,max}$	Maximum of S_{m0}
S_{max}	Maximum of S
S_{SP}	S during stable period
t	Time
t_A	Time at beginning of contact
t_B	Time at end of contact
t_C	Time of branching
T_{MC}	Metallic contact duration
V_0	Amplitude of V_0^*
V_0^*	Alternating voltage (input voltage)
V_1	Amplitude of V_1^*
V_1^*	Alternating voltage (output voltage)
Y	Yield stress
z	Vertical position
Z	Modulus of Z^*
Z_0	Z for dry condition
Z_{SP}	Z during stable period
Z^*	Complex impedance of contact
Z_t^*	Total complex impedance of circuit
α	Metallic contact ratio
α_{max}	Maximum of α
β	Radius of ball
δ	Indentation depth
Δt	Duration of contact
ε	Permittivity of lubricant
ε_0	Permittivity of vacuum
ε_r	Relative permittivity
ζ	Acceleration
η	Viscosity
θ	Argument of Z^*
θ_0	θ for dry condition
θ_{SP}	θ during stable period
π	Circular constant
σ	Resistance of metallic contact for unit area
φ	Phase difference
ω	Angular frequency

1 Introduction

When two metal surfaces collide with each other, an impact force is instantaneously generated at the contact, leading to a quite short duration of contact (e.g., 110 μ s in the experiments of the present study). In this duration, the pressure applied to the contact drastically increases, easily exceeding the pressure required for plastic deformation. To prevent surface damage occurring at the direct metal-to-metal contact (i.e., metallic contact), lubrication is generally needed.

A number of researchers have examined the effect of lubrication at short-time contacts between colliding metal surfaces. For example, Tabor [1] found that when a copper plate collides with a steel ball, a “cone-shaped indentation” is formed when the copper plate is lubricated by a paraffin oil, while a “bowl-shaped indentation” is formed when no lubricants are used. By measuring the electrical conductance of the contact during the formation of the cone-shaped indentation, it was also found that no metallic contact between the ball and plate occurs. Similar results have been found in various lubricants and materials [2–4]. In these studies, it is believed that the lubricants show the hydrodynamic lubrication effect, which is dominated by the viscosity of the lubricants.

In addition, visualizations of short-time contacts due to collisions have been conducted using optical interferometry [5–9]. Although the experiments are limited to the elastic impact on transparent targets, the temporal change observed in the profile of the lubricant film is informative and useful to investigate the behavior of the lubricant. In addition, numerical simulations have been conducted for collisions between a ball and a plate [2, 8–10] or between two cylinders [11] under lubrication. A good agreement has been found between experimental and numerical results regarding the distribution of thickness and pressure of the lubricant films.

Although many studies on the lubrication of short-time contacts have focused on the hydrodynamic effect of lubricants, a metallic contact between colliding surfaces can occur when the load capacity of the lubricant film is not sufficient to keep the surfaces separated [1–4]. In such a situation, the boundary lubrication effect of additives dissolved in the lubricants is expected to play an important role in preventing the metallic contact to reduce surface damages. In fact, the boundary lubrication effect is indispensable in industrial applications associated with collisions (e.g., metal forming processes) or impact loading (e.g., bearings and guide ways) between metal surfaces. However, the evaluation method of the boundary lubrication effect appearing at short-time contacts has not been established yet.

If not focusing on colliding surfaces, we find that the occurrence of metallic contacts (or the formation of lubricant films between metal surfaces) has been examined by using a number of electrical methods, under wet conditions lubricated by additive-free oils [12–14] and additive-containing oils [15–20]. For example, Archard and Kirk [12] measured the “resistance” and “capacitance” of a contact between rotating steel cylinders lubricated by a mineral oil, using two different circuits: a direct current (DC) circuit and an alternating current (AC) circuit, respectively. From the resistance measurements, they found that the tested lubricant remains in the contact area even at a high load, whereas from the capacitance measurements, they evaluated the film thickness. To investigate surface films formed by additives

more carefully, steel–mercury contacts have been used [15–17, 19, 20], in which the “complex impedance” of the contacts has been measured [16, 17, 19, 20]. Using an AC circuit to measure the complex impedance, we can simultaneously obtain two different physical quantities from the amplitude and phase difference responses. For example, Nakano and co-workers quantified temporal changes in the thickness and breakdown ratio of surface films formed by oiliness additives at steel–mercury contacts under quasi-static loading [17, 19, 20].

In the present study, to provide a method for investigating the transient behaviors of short-time contacts between colliding metal surfaces with a high temporal resolution, the complex impedance method was further developed, where an AC circuit with a high frequency (i.e., 500 kHz) and a high sampling rate (i.e., 20 MHz) was used. In addition, to apply the method to evaluate the boundary lubrication effect, the test lubricant was provided to one of the colliding surfaces as a homogeneous thin film, which minimized the hydrodynamic lubrication effect and therefore emphasized the boundary lubrication effect of the test lubricant. As an example, the method was applied to a simple apparatus making a short-time contact with a duration of 110 μ s occurring between a free-falling steel ball and a stationary steel plate, under the dry condition and the wet conditions lubricated by simple test lubricants consisting of representative inactive base oils (i.e., normal alkanes) and a representative oiliness additive (i.e., oleic acid), to show the availability of the developed method.

2 Experimental Details

2.1 Test Lubricants

As base oils, four types of normal alkanes [i.e., *n*-decane (D), *n*-dodecane (DD), *n*-tetradecane (TD), and *n*-hexadecane (HD)] were used. Before using them, they were percolated through molecular sieves and filtered to remove possible polar impurities. As an additive, oleic acid (OA) was used as supplied. It was dissolved in the purified base oils at a concentration of 30 mM (approximately 1 mass%). In the following sections, OA/D, OA/DD, OA/TD, and OA/HD represent 30-mM solutions of OA dissolved in D, DD, TD, and HD, respectively. The values of viscosity (temperature: 25 °C) and relative permittivity (temperature: 25 °C; frequency of alternating voltage: 500 kHz) of the test lubricants are listed in Table 1.

2.2 Apparatus

Figure 1 shows a schematic diagram of the apparatus. This apparatus employs a short-time contact between a free-falling

Table 1 Viscosity η (at 25 °C) and relative permittivity ϵ_r (at 25 °C and 500 kHz) of test lubricants

Test lubricant	η (mPa s)	ϵ_r (-)
D	0.86	2.02
DD	1.39	2.05
TD	2.11	2.05
HD	3.15	2.06
OA/D	0.89	2.02
OA/DD	1.41	2.05
OA/TD	2.16	2.05
OA/HD	3.17	2.06

D *n*-decane, *DD* *n*-dodecane, *TD* *n*-tetradecane, *HD* *n*-hexadecane, *OA* oleic acid, *OA/D* 30-mM OA solution dissolved in D, *OA/DD* 30-mM OA solution dissolved in DD, *OA/TD* 30-mM OA solution dissolved in TD, *OA/HD* 30-mM OA solution dissolved in HD

steel ball (material: AISI 52100 steel; Vickers hardness: 870; diameter: 30 mm; arithmetic average roughness: 13 nm) and a stationary steel plate (material: AISI 1045 steel; Vickers hardness: 180; dimensions: 65 mm \times 65 mm \times 5 mm; arithmetic surface roughness: 4 nm).

An electromagnet holds the ball at the initial height h_0 (=100 mm) from the upper surface of the plate mounted on the base. By turning off the electromagnet, the ball falls by gravity and collides with the plate. To detect the collision, an acceleration sensor is mounted beneath the plate. To measure the impedance at the contact under impact loading, lead wires connect the ball and plate to the electrical terminals P and Q, respectively. To minimize any mechanical disturbance to the free fall motion of the ball, a fine lead wire (diameter: 170 μ m; length: 300 mm) is used for the connection of the ball.

Figure 2 shows the electrical circuit for measuring the complex impedance of the contact between the ball and plate. An alternator (amplitude: $V_0 = 100$ mV; frequency:

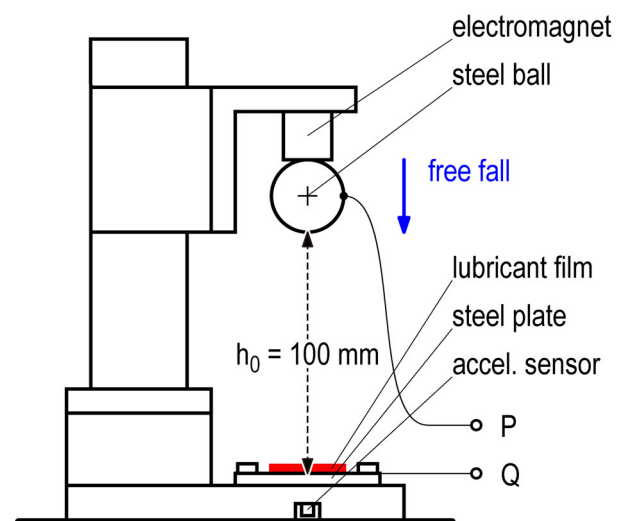


Fig. 1 Schematic diagram of apparatus

$f_0 = 500$ kHz) and a fixed resistor (resistance: $R = 50 \Omega$) are connected in series between the terminals P and Q. The coil in the figure represents the inductance $L (=3.8 \mu\text{H})$ of the circuit.

2.3 Complex Impedance of Contact

When an alternating voltage V_0^* is applied, an alternating current I_1^* passes through the circuit with a phase difference φ . They can be described in the following complex form:

$$V_0^* = V_0 \exp(j\omega t) \tag{1}$$

$$I_1^* = I_1 \exp(j(\omega t - \varphi)) \tag{2}$$

where j is the imaginary unit, t is the time, $\omega (=2\pi f_0)$ is the angular frequency, φ is the phase difference, V_0 is the amplitude of V_0^* , and I_1 is the amplitude of I_1^* . Therefore, the total complex impedance Z_t^* of the external circuit is given by

$$Z_t^* = \frac{V_0^*}{I_1^*} = \frac{V_0}{I_1} \exp(j\varphi) \tag{3}$$

Meanwhile, using R , L , and the complex impedance Z^* of the contact between the ball and plate, Z_t^* is given by

$$Z_t^* = R + j\omega L + Z^* \tag{4}$$

From Eqs. (3) and (4), we obtain

$$Z^* = \frac{V_0}{I_1} \exp(j\varphi) - R - j\omega L \tag{5}$$

The alternating voltage V_1^* between both ends of R is described by

$$V_1^* = RI_1^* = RI_1 \exp(j(\omega t - \varphi)) \tag{6}$$

Therefore,

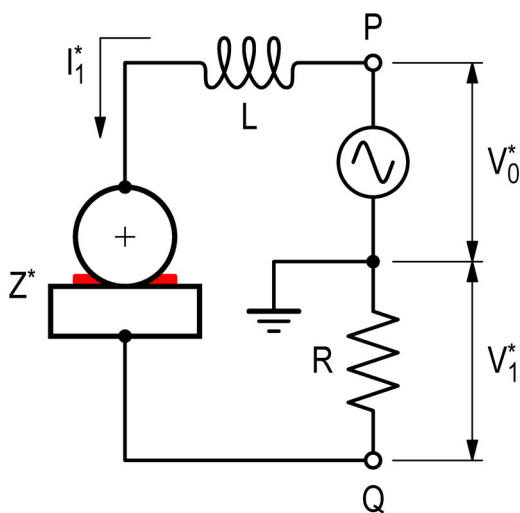


Fig. 2 Electrical circuit for measuring complex impedance Z^* of ball-plate contact

$$I_1 = \frac{V_1}{R} \tag{7}$$

$$\varphi = \arg(V_0^*) - \arg(V_1^*) \tag{8}$$

where V_1 is the amplitude of V_1^* . Consequently, from Eqs. (5), (7), and (8), we obtain

$$Z^* = R((a \cos \varphi - 1) + j(a \sin \varphi - b)) \tag{9}$$

where a and b are dimensionless coefficients, given by

$$a = \frac{V_0}{V_1} \tag{10}$$

$$b = \frac{\omega L}{R} \tag{11}$$

Therefore, the modulus and argument of Z^* are obtained by

$$Z \equiv \text{mod}(Z^*) = R\sqrt{(a \cos \varphi - 1)^2 + (a \sin \varphi - b)^2} \tag{12}$$

$$\theta \equiv \arg(Z^*) = \tan^{-1} \frac{a \sin \varphi - b}{a \cos \varphi - 1} \tag{13}$$

with the measured values of V_1 and φ .

2.4 Procedure

The steel ball and steel plate were thoroughly cleaned in acetone and in hexane using an ultrasonic cleaner and dried in a hot air stream. Then, 50 mm^3 of test lubricant was poured on the steel plate and diffused spontaneously to form a $30\text{-}\mu\text{m}$ -thick film, where the thickness was confirmed by using a laser microscope.

After installing the steel ball and steel plate, the switch of the electromagnet was turned off. The ball fell freely by gravity, collided with the lubricated portion of the plate, and rebounded vertically, where the rebounding ball was caught manually to avoid multiple collisions between the ball and plate. Using the signal from the acceleration sensor as a central trigger, temporal changes in V_0^* and V_1^* were measured simultaneously at a sampling frequency of 20 MHz for $500 \mu\text{s}$. The plastic indentation formed on the plate was observed using the laser microscope to obtain its profile. The ambient temperature and relative humidity range were $25 \text{ }^\circ\text{C}$ and $20\text{--}40 \%$, respectively.

3 Results and Discussion

3.1 Indentation Formed on Steel Plate

Figure 3 shows typical examples of the indentation central profiles formed on the steel plate for the dry (blue line) and

wet (red line) conditions, with OA/HD used as lubricant for the wet condition. The black line shows the central profile of the steel ball. The radial origin ($r = 0$) shows the central position of the indentation, and the vertical origin ($z = 0$) shows the initial surface profile of the steel plate before the collision.

We found that both indentations present a bowl-type shape with marked shoulders, and they are quite similar: For both conditions, the diameter and depth of the indentation are 2.0 mm and 15 μm , respectively. This means that the OA/HD film has little hydrodynamic lubrication effect, probably due to its low viscosity (i.e., $\eta = 3.17 \text{ mPa s}$ at 25 $^\circ\text{C}$) and reduced initial thickness (i.e., 30 μm). It should be noted that the indentation profiles deviate from the ball profile (i.e., the circle with a diameter of 30 mm) probably due to the elastic recovery of the steel ball and steel plate occurring during the rebound process. It should also be noted that quite similar profiles were obtained for all the other test lubricants (i.e., D, DD, TD, HD, OA/D, OA/DD, and OA/TD). In other words, we cannot judge whether the test lubricants have any lubrication effects in the considered experimental conditions, at least based on the appearance of plastic indentations.

3.2 Temporal Change in Complex Impedance

Figure 4 shows typical examples of temporal change in the acceleration ζ (green line) and temporal changes in the input voltage V_0^* (blue line) and output voltage V_1^* (red line)

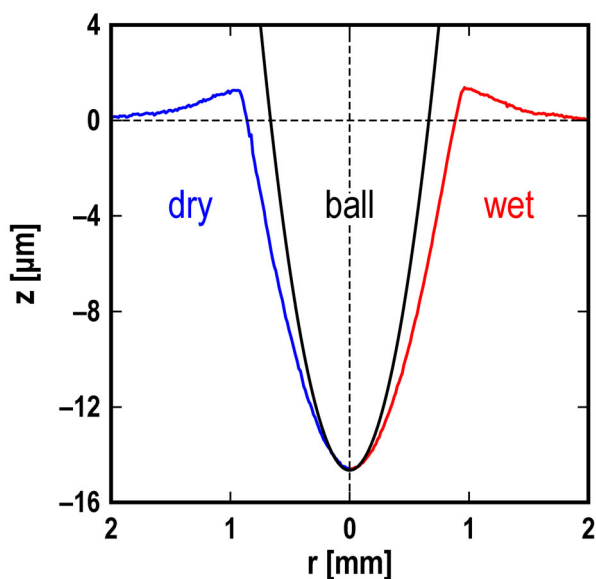


Fig. 3 Indentation central profiles formed on steel plate; *blue line*: dry condition; *red line*: wet condition (lubricant: OA/HD); *black solid line*: central profile of steel ball (diameter: 30 mm) (Color figure online)

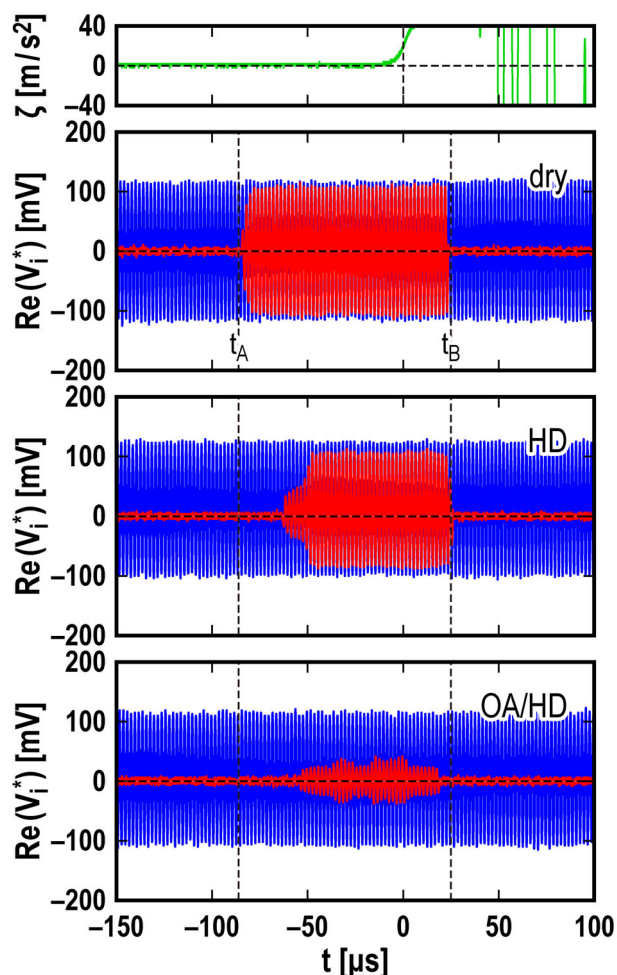


Fig. 4 Typical examples of temporal change in acceleration ζ (*green line*) and temporal changes in input voltage V_0^* (*blue line*) and output voltage V_1^* (*red line*) for dry condition, wet condition (lubricant: HD), and wet condition (lubricant: OA/HD) (Color figure online)

for the dry condition, wet condition lubricated by HD, and wet condition lubricated by OA/HD. The origin of the abscissa ($t = 0$) represents the time when the acceleration sensor mounted beneath the plate responded to the collision between the ball and plate, where the threshold value $\zeta = 20 \text{ m/s}^2$ was used. The vertical broken lines at $t = t_A$ ($= -85 \mu\text{s}$) and t_B ($= 25 \mu\text{s}$) show the beginning and end of the contact, respectively, as will be explained in Fig. 5. From these temporal changes in V_0^* and V_1^* , temporal changes in Z [Eq. (12)] and θ [Eq. (13)] were calculated by using the short-time Fourier transformation method, where the window width and window shift were 4 and 2 μs , respectively.

Figure 5 shows the temporal changes in Z and θ for the dry condition (black circles), wet condition lubricated by HD (blue circles), and wet condition lubricated by OA/HD (red circles), calculated from the experimental data shown in Fig. 4. For every condition, the time rate of change in Z clearly changes at $t = t_A$ and $t = t_B$, which means that

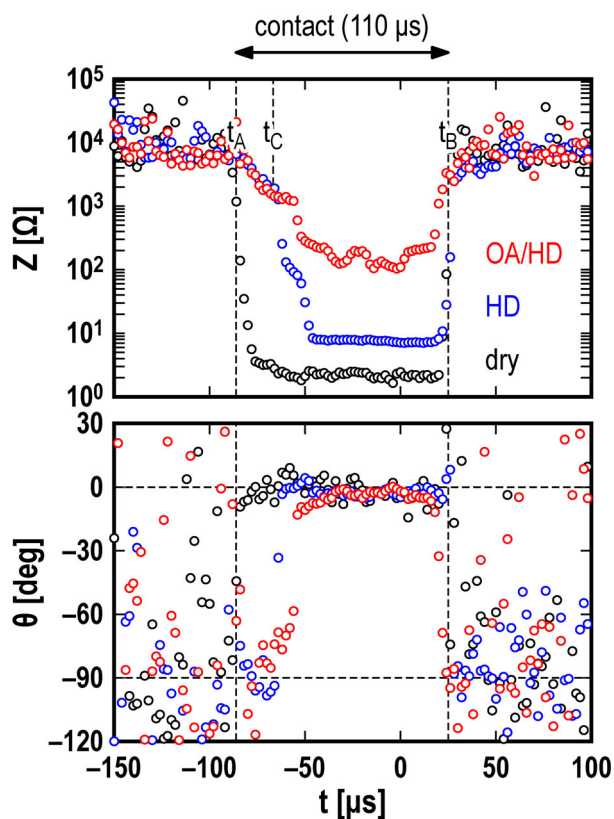


Fig. 5 Temporal changes in modulus Z and argument θ of complex impedance Z^* of ball-plate contact; *black circles*: dry condition; *blue circles*: wet condition (lubricant: HD); *red circles*: wet condition (lubricant: OA/HD) (Color figure online)

the metallic contact began at $t = t_A$ and ended at $t = t_B$. Thus, the contact duration is $110 \mu s (=t_B - t_A)$, where the lubrication conditions have little effect on the contact duration, which is consistent to the results found for the plastic indentations, whose shapes are not affected by the lubrication conditions.

In the dry condition, before the contact (i.e., $t < t_A$), the Z values are around $10^4 \Omega$ and the θ values appear to be scattered. This corresponds to the situation, in which the ball and plate are separated by a sufficiently large distance. In this situation, as shown in Fig. 4, the signal of V_1^* is weak, which makes it difficult to determine the phase difference between V_0^* and V_1^* accurately, leading to the scattered values of θ with large errors from the theoretical value $\theta = -90^\circ$. Then, from $t = t_A$, Z starts to decrease and θ to increase. After $30 \mu s$, both appear to be stable with mean values of $Z_{SP} = 2.2 \Omega$ and $\theta_{SP} = -1.2^\circ$, and this state is maintained for $75 \mu s$. After this stable period, Z increases and θ decreases, both rapidly, for $5 \mu s$. After the contact (i.e., $t > t_B$), Z and θ are at the initial values, the same they showed before the contact.

In the wet condition lubricated by the additive-free base oil HD, temporal changes in Z and θ resemble

those observed in the dry condition. However, the falling rate of Z after $t = t_A$ is lower than that registered in the dry condition. The mean value of Z during the stable period is $Z_{SP} = 8.8 \Omega$, several times higher than those recorded in the dry condition. The mean value of θ during the stable period is $\theta_{SP} = -2.6^\circ$, indicating the presence of a lubricant film in the contact.

In the wet condition lubricated by the additive-containing oil OA/HD, the falling behavior of Z after $t = t_A$ resembles at first the one observed for HD. However, at $t = t_C (= -65 \mu s)$, the temporal change in Z for OA/HD appears to start to deviate upward from that for HD. The mean values of Z and θ during the stable period are $Z_{SP} = 170 \Omega$ and $\theta_{SP} = -3.8^\circ$, respectively, indicating the presence of a thicker lubricant film in the contact than the case for HD.

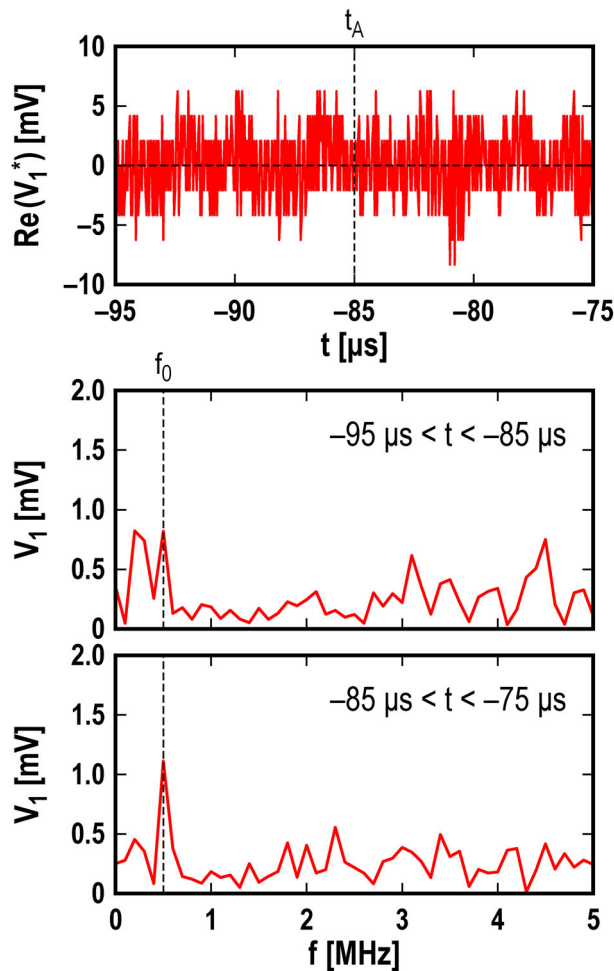


Fig. 6 Magnification of temporal change in V_1^* for wet condition (lubricant: HD) and spectra for former half part ($-95 \mu s < t < -85 \mu s$) and latter half part ($-85 \mu s < t < -75 \mu s$)

Note that the beginning of the contact at $t = t_A$ is clear in Fig. 5, although it is unclear in Fig. 4 for the two lubricated conditions (i.e., for the wet conditions lubricated by HD and OA/HD). This is an advantage of using the complex impedance measurement with a high-frequency AC circuit, in which by using spectrum analysis (e.g., the Fourier transformation method), the amplitude at the frequency f_0 of the alternator can be extracted from a weak signal of the output voltage V_1^* , as Fig. 6 shows for the wet condition lubricated by HD. This leads to the bending points of the function $Z = Z(t)$ at $t = t_A$ and t_B in Fig. 5, which tells us clearly when the contact began and ended.

3.3 Mean Contact Pressure in Short-time Contact

Let us evaluate the value of the mean contact pressure \bar{P} during the short-time contact. Based on the conservation of momentum, the mean contact force \bar{F} is given by

$$\bar{F} = \frac{m(1 + e_r)\sqrt{2gh_0}}{\Delta t} \tag{14}$$

where g is the gravitational constant, m is the mass of the ball, h_0 is the initial height of the ball, Δt is the duration of the contact, and e_r is the coefficient of restitution. Therefore, we obtain the value of the mean contact force $\bar{F} = 2.4$ kN by using the following values: $g = 9.81$ m/s², $m = 0.11$ kg, $h_0 = 100$ mm, $\Delta t = 110$ μ s, and $e_r = 0.69$, where the value of e_r was measured experimentally, which was invariant for all the lubrication conditions. Based on the indentation shapes shown in Fig. 3, if we take 1 mm² as the representative value of the apparent contact area during the short-time contact, we can estimate the mean contact pressure as $\bar{P} = 2.4$ GPa, which is quite close to the value of the plastic flow pressure of the plate material (i.e., $p_p \sim 3Y = 2.2$ GPa, where p_p is the plastic flow pressure and $Y = 0.73$ GPa is the yield stress of AISI 1045 steel).

3.4 Interpretation of Measured Complex Impedance

3.4.1 Metallic Contact Ratio

In this section, we focus on the interpretation of the measured complex impedance shown in Fig. 5.

Assume that the complex impedance Z^* of the contact is a function of the resistance R_m of the metallic contact and the capacitance C_f of the air film (for the dry condition) or lubricant film (for the wet conditions).

$$Z^* = (R_m^{-1} + j\omega C_f)^{-1} \tag{15}$$

Let S , S_m , and S_f be the apparent contact area, the metallic contact area, and the area covered with the film, respectively; that is,

$$S = S_m + S_f \tag{16}$$

In addition, for simplicity, assuming that the film is homogeneous with a thickness d , we obtain

$$R_m = \frac{\sigma}{S_m} \tag{17}$$

$$C_f = \frac{\epsilon S_f}{d} \tag{18}$$

where σ is the resistance of the metallic contact for unit area and ϵ is the permittivity of the film. From the above equations, we obtain

$$S_m = \frac{\sigma \cos \theta}{Z} \tag{19}$$

$$d = -\frac{\epsilon \omega Z(S - S_m)}{\sin \theta} \tag{20}$$

Note that in theory, since θ ranges from -90° to 0° , the value of d obtained from Eq. (20) becomes positive.

It is natural to assume that the maximum of the metallic contact area S_m appears in the dry condition. Therefore, from Eq. (19), we obtain

$$\alpha \equiv \frac{S_m}{S_{m0,max}} = \frac{Z^{-1} \cos \theta}{\max(Z_0^{-1} \cos \theta_0)} \tag{21}$$

where α is termed as the metallic contact ratio and the subscript 0 in Eq. (21) means that the value is for the dry condition. Consequently, by using Eq. (21), we can

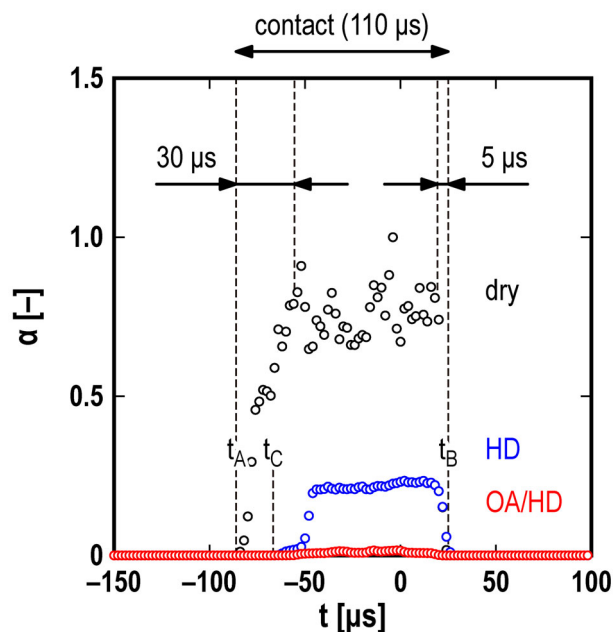


Fig. 7 Temporal change in metallic contact ratio α calculated from measured complex impedance of ball-plate contact; *black circles*: dry condition; *blue circles*: wet condition (lubricant: HD); *red circles*: wet condition (lubricant: OA/HD) (Color figure online)

calculate the instantaneous value of α with the measured values of Z and θ .

Figure 7 shows the temporal change in α obtained from the temporal changes in Z and θ shown in Fig. 5, which tells us the following behaviors of the short-time contact.

First, from the temporal change in α for the dry condition, we find that in the first 30 μs , α increases from zero at a mean rate of $0.03 \mu\text{s}^{-1}$. In the following 75 μs , α keeps high values with variations in the range from 0.65 to 1.00. Then, in the final 5 μs , α decreases drastically at a mean rate of $-0.16 \mu\text{s}^{-1}$. The difference in the mean rate between the first 30 μs and the final 5 μs results in the asymmetric shape of the temporal change, which must be caused by the difference between the elastoplastic deformation occurring in the approach period and the elastic deformation occurring in the departure period.

Then, from the temporal change in α for the wet condition lubricated by HD, we find that compared with the dry condition, the considerable growth of α in the approach period is delayed by 20 μs and suppressed to 0.23. This means that the 77 % of the maximum metallic contact area of the dry condition is reduced by a residual film of HD, which failed to be squeezed out of the contact, probably due to its viscosity.

Finally, from the temporal change in α for the wet condition lubricated by OA/HD, we find that the growth of α is mostly suppressed to 0.02. Considering that the bulk viscosity of OA/HD (i.e., $\eta = 3.17 \text{ mPa s}$ at 25 °C) is almost the same as that of HD (i.e., $\eta = 3.15 \text{ mPa s}$ at 25 °C), we can say that the boundary lubrication effect due to the 30-mM OA dissolved in HD suppresses the breakdown of the residual film and reduces the metallic contact in the short-time contact, not the hydrodynamic effect due to OA/HD.

3.4.2 Residual Film Thickness

Plotting the metallic contact ratio α shown in Fig. 7 against the modulus Z , we obtain the graph shown in Fig. 8. When $\alpha > 10^{-3}$, we find that most of the data are plotted on a single straight line with a slope of -1 . This means that when estimating α , the modulus Z is dominant, and thus, the effect of the argument θ is small. However, using the value of θ , we can estimate the thickness of the residual film appearing in the stable period as follows.

It is natural to assume that the maximum of the apparent contact area S appears in the stable period. In addition, considering that the lubrication conditions have little effect on the indentation shape shown in Fig. 3, we can assume that the maximum of S (i.e., S_{max}) is invariant for all lubrication conditions. In the following, S_{max} is approximated by the spherical cap of the steel ball, where the height of the spherical cap is approximated by the depth of the plastic indentation formed on the steel plate. Then, S_{max} is given by

$$S_{\text{max}} = 2\pi\beta\delta \tag{22}$$

where β (=15 mm) is the radius of the steel ball and δ (=15 μm) is the indentation depth shown in Fig. 3, leading to the value $S_{\text{max}} = 1.4 \text{ mm}^2$. Consequently, the residual film thickness d_{min} is given by

$$d_{\text{min}} = -\frac{\varepsilon\omega Z_{\text{SP}}(S_{\text{SP}} - S_{\text{m,SP}})}{\sin \theta_{\text{SP}}} \simeq -\frac{\varepsilon\omega Z_{\text{SP}}(S_{\text{max}} - S_{\text{m,max}})}{\sin \theta_{\text{SP}}} \tag{23}$$

where the subscript SP means that the value is for the stable period. Using the maximum of α given by

$$\alpha_{\text{max}} = \frac{S_{\text{m,max}}}{S_{\text{m0,max}}} \tag{24}$$

we obtain

$$d_{\text{min}} = -\left(1 - \frac{S_{\text{m0,max}}}{S_{\text{max}}} \alpha_{\text{max}}\right) \frac{\varepsilon\omega Z_{\text{SP}} S_{\text{max}}}{\sin \theta_{\text{SP}}} \tag{25}$$

Since $0 < S_{\text{m0,max}} < S_{\text{max}}$, we obtain

$$-(1 - \alpha_{\text{max}}) \frac{\varepsilon\omega Z_{\text{SP}} S_{\text{max}}}{\sin \theta_{\text{SP}}} < d_{\text{min}} < -\frac{\varepsilon\omega Z_{\text{SP}} S_{\text{max}}}{\sin \theta_{\text{SP}}} \tag{26}$$

Using the values of α_{max} and parameters (i.e., $\varepsilon = \varepsilon_r \varepsilon_0$ F/m, $\omega = 2\pi \times 0.5 \times 10^6$ rad/s, and $S_{\text{max}} = 1.4 \text{ mm}^2$, where ε_r is the relative permittivity and $\varepsilon_0 (=8.85 \times 10^{-12}$ F/m) is the permittivity of vacuum), we obtain the values of d_{min} listed in Table 2.

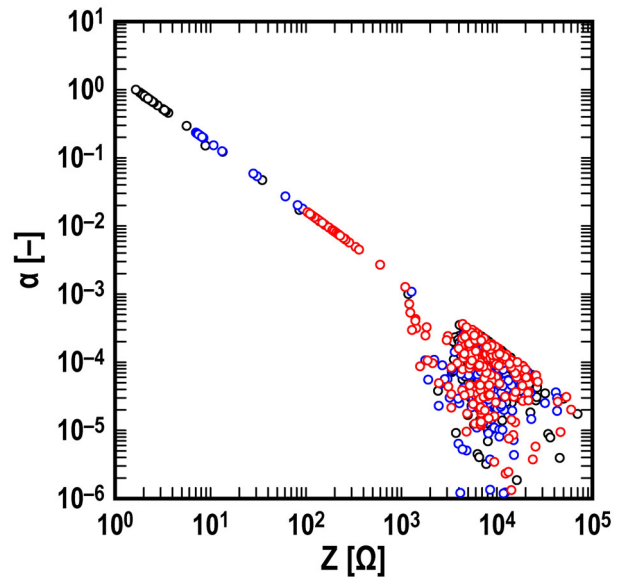


Fig. 8 Relationship between metallic contact ratio α and modulus Z of ball-plate contact; black circles: dry condition; blue circles: wet condition (lubricant: HD); red circles: wet condition (lubricant: OA/HD) (Color figure online)

Table 2 Maximum metallic contact ratio (α_{\max}) and residual film thickness (d_{\min}) estimated from measured values shown in Fig. 5

Lubrication condition	α_{\max} (-)	d_{\min} (nm)
Dry (air)	1.00	0–4
Wet (HD)	0.23	12–16
Wet (OA/HD)	0.02	200

Note that the estimated value of the residual film thickness d_{\min} for the wet condition lubricated by OA/HD (i.e., $d_{\min} = 200$ nm in two-digit accuracy) is considerably higher than that for HD (i.e., $12 \text{ nm} < d_{\min} < 16$ nm in two-digit accuracy). Considering that the bulk viscosity of OA/HD (i.e., $\eta = 3.17$ mPa s at 25°C) is almost the same as that of HD (i.e., $\eta = 3.15$ mPa s at 25°C), we can say that the boundary lubrication effect due to the 30-mM OA dissolved in HD thickens the residual film, not the hydrodynamic effect due to OA/HD. It is also noted that although the value $d_{\min} = 200$ nm for OA/HD is sufficiently higher than the surface roughnesses of the ball (arithmetic average roughness: 13 nm) and plate (arithmetic average roughness: 4 nm), the positive value $\alpha_{\max} = 0.02$ for OA/HD demonstrates the occurrence of a metallic contact. This can be attributed to the eventual high asperities preexisting on the surfaces of the ball (maximum peak height: 320 nm) and plate (maximum peak height: 170 nm).

3.5 Evaluation of Lubrication Effect at Short-time Contact

In addition to the three lubrication conditions described above (i.e., dry condition and wet conditions lubricated by HD and OA/HD), also for the other six lubrication conditions (i.e., wet conditions lubricated by D, DD, TD, OA/D, OA/DD, and OA/TD), temporal changes in the complex impedance [i.e., $Z(t)$ and $\theta(t)$ like Fig. 5] were obtained experimentally and then temporal changes in the metallic contact ratio [i.e., $\alpha(t)$ like Fig. 7] were calculated in the same manner. In this section, to evaluate the lubrication effect at the short-time contact, we introduce a new measure: the metallic contact duration T_{MC} , which is defined as the time duration for $\alpha > 0.01$.

Figure 9 shows the values of T_{MC} for all the nine lubrication conditions, where the columns and error bars represent the mean values and standard deviations of ten measurements, respectively. In the dry condition (represented by a black column), the mean value of T_{MC} is $110 \mu\text{s}$. On the other hand, in the wet conditions lubricated by base oils (i.e., D, DD, TD, and HD represented by blue columns), the mean values of T_{MC} are around $90 \mu\text{s}$, more than 10 % lower than for the dry condition. Since these

base oils do not contain any surface active agents, the observed decrease in T_{MC} can be attributed to the hydrodynamic lubrication effect of the base oils during the short-time contact, although the values are close to one another and do not depend on the viscosity, probably due to the small initial thickness (i.e., $30 \mu\text{m}$).

However, in the wet conditions lubricated by additive-containing oils (i.e., OA/D, OA/DD, OA/TD, and OA/HD represented by red columns), a clear dependence of T_{MC} on the selected base oil is found, as shown in Fig. 9. As the number of carbon atoms in a single molecule of base oil increases, T_{MC} decreases monotonically. For example, for OA/D, the mean value of T_{MC} is close to that of the base oil D, whereas for OA/HD, it is $50 \mu\text{s}$, which is approximately 50 % lower than that of the base oil HD. Since the viscosity of OA/HD (i.e., $\eta = 3.17$ mPa s at 25°C) is quite close to that of HD (i.e., $\eta = 3.15$ mPa s at 25°C), the observed decrease in the mean value of T_{MC} should be attributed to the boundary lubrication effect of OA, and not to the hydrodynamic lubrication effect. Therefore, we can conclude that the boundary lubrication effect of OA used as an additive during a short-time contact of the duration of $110 \mu\text{s}$ depends strongly on the chain length of the normal alkanes used as base oils.

This reminds us of the chain-matching effect firstly reported by Cameron et al. [21]. With systematic experiments on the lubricated sliding friction performed using a four-ball apparatus, they found that when the base oil and additive have the same chain length and shape, a sharp peak appears in the curve of the scuffing load for each base oil as a

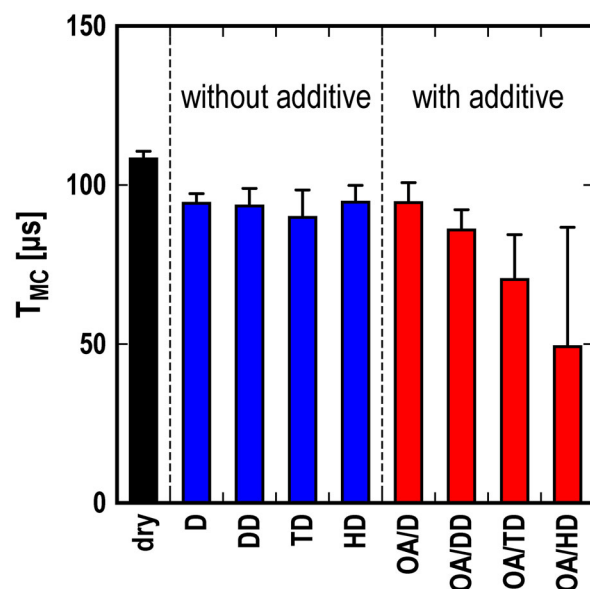


Fig. 9 Metallic contact duration T_{MC} (for $\alpha > 0.01$) for different lubrication conditions; column and error bar: mean value and standard deviation of ten measurements, respectively

function of the chain length of additives. Using a squeeze film apparatus, Askwith et al. [22] found that the effective viscosity of fatty acid solutions in *n*-hexadecane at a thickness of 2 μm shows the maximum value when *n*-hexadecanoic acid is used, which indicates that the effective viscosity at a small thickness causes the chain-matching effect. The chain-matching effect also appears in the variation of the transition temperature, defined as the temperature at which the friction coefficient of a lubricated sliding contact increases sharply [23, 24]. This has been explained by the changes occurring in the adsorption heat and entropy [25–27]. So far, the chain-matching effect has been examined based on the residual film thickness under hydrostatic pressure [16, 26, 28], change in the freezing temperature [29, 30], and change in the freezing pressure [30]. In the present study, since *n*-octadecane is solid at the ambient temperature (i.e., 25 °C), it was impossible to use it as a base oil, and this was possibly the reason why the T_{MC} values for additive-containing oils were found monotonic with no minimum. However, the fact that the chain length of the base oils has an effect, not on the T_{MC} values of the base oils, but on the T_{MC} values of the additive-containing oils, can be attributed to the mechanisms related to the chain-matching effect, as explained above, although the surface protection provided by the additive (i.e., oleic acid) appeared at a short-time contact within 110 μs .

It should be noted that when the additive-containing oils were used, relatively large standard deviations of T_{MC} were observed, as the error bars in Fig. 9 show. These large standard deviations can be attributed to the nonuniformity of the surface topography. A local contact between eventual high asperities can easily cause a local breakdown of the surface films. Even if the local breakdown area is small, it makes the standard deviation of T_{MC} large, which makes the phenomenon stochastic. We can say that the ten measurements collected in this experiment were sufficient to cover the stochastic event mentioned above and to lead to systematic results on the mean value of T_{MC} , as shown in Fig. 9.

4 Conclusions

The complex impedance method was developed for investigating the transient behaviors of short-time contacts between colliding steel surfaces, by using an AC circuit with a high frequency of 500 kHz at a high sampling rate of 20 MHz. The method was applied to estimating the lubrication effects of simple test lubricants acting at a short-time contact with a duration of 110 μs occurring between a free-falling steel ball and a stationary steel plate, where to minimize the hydrodynamic lubrication effect, the test lubricant was provided on the steel plate as a

homogeneous thin film with a thickness of 30 μm . The main conclusions drawn from the results are as follows:

1. The modulus Z of the complex impedance of the short-time contact can detect the beginning and end of the contact with high accuracy, even though they are apparently unclear in the output voltage signal from the circuit, especially for wet conditions.
2. Using the modulus Z and argument θ of the complex impedance of the short-time contact, the metallic contact ratio α (defined as the ratio of the metallic contact area for a lubrication condition to the maximum metallic contact area for the dry condition) and the residual film thickness d_{min} can be obtained quantitatively.
3. The complex impedance of the short-time contact can clarify the differences in the lubrication effects of lubricants, even though the differences in the lubricants do not change the shape of the plastic indentation formed on the steel plate. For example, at the short-time contact, the metallic contact duration T_{MC} (defined as the time duration for $\alpha > 0.01$) quantified the differences in the boundary lubrication effects of the selected base oils (i.e., *n*-decane, *n*-dodecane, *n*-tetradecane, and *n*-hexadecane) and the 30-mM oleic acid solutions dissolved in the base oils.

References

1. Tabor, D.: Collisions through liquid layers. *Engineering* **167**, 145–147 (1949)
2. Christensen, H.: The oil film in a closing gap. *Proc. Roy. Soc. Lond.* **A266**, 312–328 (1962)
3. Imado, K., Miyagawa, H., Miura, A., Ueyama, N., Hirano, F.: Behavior of traction oils under impact loads. *Tribol. Trans.* **37**, 378–386 (1994)
4. Ohno, N., Rahman, M.Z., Tsutsumi, H.: High-pressure short time behavior of traction fluids. *Lubr. Sci.* **18**, 25–36 (2006)
5. Dowson, D., Jones, D.A.: Lubricant entrapment between approaching elastic solids. *Nature* **214**, 947–948 (1967)
6. Safa, M.M.A., Gohar, R.: Pressure distribution under a ball impacting a thin lubricant layer. *Trans. ASME* **108**, 372–376 (1986)
7. Larsson, R., Lundberg, J.: Study of lubricated impact using optical interferometry. *Wear* **190**, 184–189 (1995)
8. Kaneta, M., Ozaki, S., Nishikawa, H., Guo, F.: Effects of impact loads on point contact elastohydrodynamic lubrication films. *Proc. Inst. Mech. Eng.* **J221**, 271–278 (2007)
9. Kaneta, M., Nishikawa, H., Mizui, M., Guo, F.: Impact elastohydrodynamics in point contacts. *Proc. Inst. Mech. Eng.* **J225**, 1–12 (2011)
10. Dowson, D., Wang, D.: An analysis of the normal bouncing of a solid elastic ball on an oily plate. *Wear* **179**, 29–37 (1994)
11. Lee, K.M., Cheng, H.S.: The pressure and deformation profiles between two normally approaching lubricated cylinders. *Trans. ASME* **95**, 308–317 (1973)
12. Archard, J.F., Kirk, M.T.: Lubrication at point contacts. *Proc. Roy. Soc. Lond.* **A261**, 532–550 (1961)
13. Hamilton, G.M., Moore, S.L.: Deformation and pressure in an elastohydrodynamic contact. *Proc. Roy. Soc. Lond.* **A322**, 313–330 (1971)

14. Ten Napel, W.E., Bosma, R.: The influence of surface roughness on the capacitive measurement of film thickness in elastohydrodynamic contacts. *Proc. Inst. Mech. Eng.* **185**, 635–639 (1970)
15. Smith, A.J., Cameron, A.: Rigid surface films. *Proc. Roy. Soc. Lond.* **A328**, 541–560 (1972)
16. Okabe, H., Watanabe, Y.: Thin residual films between steel–mercury surfaces. *ASLE Trans.* **25**, 33–38 (1982)
17. Nakano, K., Akiyama, Y.: Simultaneous measurement of film thickness and coverage of loaded boundary films with complex impedance analysis. *Tribol. Lett.* **22**, 127–134 (2006)
18. Lord, J., Larsson, R.: Film-forming capability in rough surface EHL investigated using contact resistance. *Tribol. Int.* **41**, 831–838 (2008)
19. Manabe, K., Nakano, K.: Breakdown of oil films and formation of residual films. *Tribol. Int.* **41**, 1103–1113 (2008)
20. Nakano, K., Manabe, K.: Breakdown processes of boundary films formed by oiliness additives. *Tribol. Online* **6**, 277–283 (2011)
21. Cameron, A., Crouch, R.F.: Interaction of hydrocarbon and surface-active agent. *Nature* **198**, 475–476 (1963)
22. Askwith, T.C., Cameron, A., Crouch, R.F.: Chain length of additives in relation to lubricants in thin film and boundary lubrication. *Proc. Roy. Soc. Lond.* **A291**, 500–519 (1966)
23. Grew, W., Cameron, A.: Friction transition temperature effect of matching surfactant and carrier. *Nature* **214**, 429–430 (1967)
24. Grew, W., Cameron, A.: Role of austenite and mineral oil in lubricant failure. *Nature* **217**, 481–482 (1968)
25. Grew, W.J.S., Cameron, A.: Thermodynamics of boundary lubrication and scuffing. *Proc. Roy. Soc. Lond.* **A327**, 47–59 (1972)
26. Cameron, A., Day, R.S., Sharma, J.P., Smith, A.J.: Studies in interaction of additive and base stock. *ASLE Trans.* **19**, 195–200 (1976)
27. Cameron, A.: The role of surface chemistry in lubrication and scuffing. *ASLE Trans.* **23**, 388–392 (1980)
28. Okabe, H., Kanno, T.: Behavior of polar compounds in lubricating-oil films. *ASLE Trans.* **24**, 459–466 (1981)
29. Okabe, H., Masuko, M., Sakurai, K.: Dynamic behavior of surface-adsorbed molecules under boundary lubrication. *ASLE Trans.* **24**, 467–473 (1981)
30. Hirano, F., Sakai, T., Kuwano, N., Ohno, N.: Chain matching between hydrocarbon and fatty acid as interfacial phenomena. *Tribol. Int.* **20**, 186–204 (1987)